Journal of
Testing and Evaluation

Hans-Jakob Schindler[1] and Dietmar Kalkhof[2]

DOI: 10.1520/JTE20120321

A Closer Look at Effects of the Loading Rate on Fracture Toughness in the Ductile-to-Brittle Transition Regime of a Ferritic Steel

VOL. 43 / NO. 3 / MAY 2015

Journal of Testing and Evaluation

doi:10.1520/JTE20120321 / Vol. 43 / No. 3 / May 2015 / available online at www.astm.org

Hans-Jakob Schindler[1] and Dietmar Kalkhof[2]

A Closer Look at Effects of the Loading Rate on Fracture Toughness in the Ductile-to-Brittle Transition Regime of a Ferritic Steel

Reference

Schindler, Hans-Jakob and Kalkhof, Dietmar , "A Closer Look at Effects of the Loading Rate on Fracture Toughness in the Ductile-to-Brittle Transition Regime of a Ferritic Steel," *Journal of Testing and Evaluation*, Vol. 43, No. 3, 2015, pp. 1–10, doi:10.1520/JTE20120321. ISSN 0090-3973

ABSTRACT

An increased loading rate causes not only a shift of the ductile-to-brittle transition curve, but also a slight change of the shape of this curve. The latter tends to become steeper as the loading rate increases. This effect was observed even at loading rates that are considered to be quasi-static according to ASTM E1921 [ASTM E1921-13: Standard Test Method for Determination of Reference Temperature, T_0, for Ferritic Steels in the Transition Range, *Annual Book of ASTM Standards*, ASTM International, West Conshohocken, PA, 2013. Actually, the coefficient 0.019 in the exponent of the MC turned out to be substantially higher at elevated loading rates. This means that a basic assumption of the evaluation procedure of ASTM E1921 is not met, which leads to an increased uncertainty of T_0 or $T_{0,x}$, respectively. This effect of is most pronounced in testing at elevated loading rates using the single-temperature option. An improved method to determine the reference temperature is proposed, where the exponent in the median transition curve in ASTM E1921 is considered to be an open parameter. The resulting reference temperatures, denoted as T_{100} and $T_{100,x}$, respectively, are expected to be more accurate than standard T_0, which is confirmed by comparison with experimental data. Furthermore, the validity requirements for T_{100} are less restrictive and more suitable than those in ASTM E1921, since they do not depend on the outcome of the tests. Based on the improved data, an improved estimation formula for the rate-induced shift of T_0 is derived. Suggestions are made for improvement of ASTM E1921.

Keywords

reference temperature, ferritic steel, loading rate, temperature shift, ductile-to-brittle transition, master curve

Manuscript received November 6, 2012; accepted for publication March 21, 2014; published online October 10, 2014.

[1] Mat-Tec AG, Unterer Graben 27, 8401 Winterthur, Switzerland, e-mail: schindler@mat-tec.ch

[2] Swiss Federal Nuclear Safety Inspectorate (ENSI), Industriestrasse, 5200 Brugg, Switzerland.

Introduction

The fracture behavior of ferritic steels is characterized by a steep drop of fracture toughness K_{Ic} in a relatively narrow temperature range, the so-called ductile-to-brittle transition (DBT). In the DBT-regime K_{Ic} exhibits a high sensitivity not only to temperature, but also to further influencing influences such as loading rate, component size, and crack-tip constraints. Furthermore, for physical reasons, it is affected by an inherent scatter, so statistical approaches are required in this toughness regime. The transition curve, as qualitatively sketched in **Fig. 1**, represents the median K_{Jc} values of the scatter band. Its location on the temperature axis can be described by the reference temperature T_0 as defined in ASTM E1921 [1].

It is commonly known that the DBT-regime is shifted to higher temperatures if the loading rate is increased (**Fig. 1**). The physical reason for this behavior is the dependence of the yield stress on the strain rate [2]. Correspondingly, low- and medium-strength steels exhibit a more pronounced rate sensitivity than high-strength steel, because the latter have a reduced capacity of strain rate hardening. The following empirical estimation formula for the temperature shift between quasi-static loading and the loading rate that corresponds to a standard Charpy test [3] was suggested by Rolfe and Barsom [4]:

$$\Delta T_{\mathrm{R\&B}}[^{\circ}\mathrm{C}] = 119 - 0.12 \cdot R_{p0.2}[\mathrm{MPa}] \tag{1}$$

In Eq 1, $R_{p0.2}$ is the static yield strength (in MPa) at room temperature. Based on Ref 5, the following semi-empirical relation to estimate the reference temperature $T_{0,x}$ under an increased loading rate $\dot{K}_I$ is provided in Ref 1:

$$T_{0,x}[^{\circ}\mathrm{C}] = \frac{(T_0 + 273.15)\cdot\Gamma}{\Gamma - \ln \dot{K}_I} - 273.15 \tag{2a}$$

where:

$$\Gamma = 9.9 \cdot \exp\left\{\left[\frac{T_0 + 273.15}{190}\right]^{1.66} + \left(\frac{R_{p0.2}(T_0)}{722}\right)^{1.09}\right\} \tag{2b}$$

FIG. 1 Shift and distortion of transition curve (schematic).

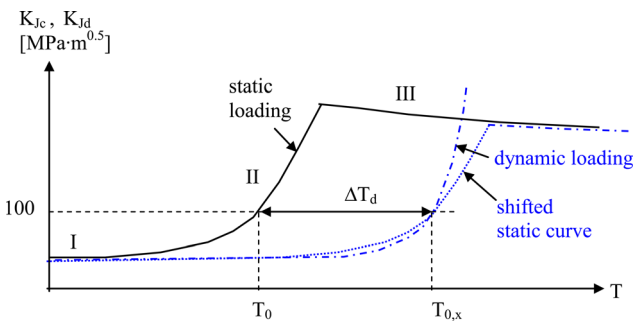

Following the nomenclature of Ref 1, $T_{0,x}$ denotes the reference temperature T_0 under an elevated loading rate, where x indicates the loading rate ($x = \log \dot{K}_I$ rounded to the integer). $R_{p0.2}(T_0)$ is the yield strength at $T = T_0$.[3]

As noted in Ref 6, there are experimental indications as well as physical reasons to assume that an increased loading rate causes not only a shift of the DBT temperature, but also a certain distortion of the DBT curve. The transition curve under dynamic loading is somewhat steeper then in the case of static loading, as sketched in **Fig. 1**. Compared with the temperature-shift quantified by Eqs 1 or 2, this can be considered as a rate effect of second order. Nevertheless, it still can be of practical significance, as explained below.

The procedure to evaluate T_0 according to Ref 1 is based on the assumption that the transition curve of a standard $1T$ specimen (i.e., thickness $B = 25.4$ mm) of ferritic steel follows the "master-curve" (MC).

$$K_{\mathrm{Jcmed}(1T)} = 30 + 70 \cdot \exp[0.019 \cdot (T - T_0)] \tag{3}$$

in the temperature range $T_0 - 50\,\mathrm{K} < T < T_0 + 50\,\mathrm{K}$ [1]. T_0, the only material-dependent parameter in Eq 3, has to be determined experimentally from a sufficient number of K_{Jc} tests in the DBT range. According to Ref 1, tests performed at elevated loading rates can be evaluated in the same way. The corresponding reference temperature is denoted as $T_{0,x}$. Evidently a distortion of the curve described by Eq 3 affects the resulting $T_{0,x}$.[4]

To quantify the measurement uncertainty of $T_{0,x}$, the Swiss Federal Nuclear Safety Inspectorate (ENSI) sponsored a research project to investigate the effect of possible influencing factors such as specimen size, specimen type, loading rate and test temperature. Briefly, the findings are presented in Refs 7 and 8. Concerning the effect of the loading rate, it is shown experimentally that there is a rate-induced distortion of the transition curve and theoretical considerations suggest that it can have a detrimental effect on $T_{0,x}$. In the present paper, this issue is treated in more depth and detail. A possibility of how to account for this effect in the evaluation of $T_{0,x}$ is suggested. Furthermore, a semi-empirical formula similar to Eq 2 is derived to estimate the effect of the loading rate on the reference temperature.

Experimental Data

A detailed description of the tests can be found in Refs 9 and 10, so only a short overview is given here. Various specimen

[3]Note that Eq 2 performs better if the yield stress at room temperature, not at T_0, is used in Eq 2*b*. Actually, according to the corresponding background paper [5] $\sigma_{\mathrm{YS}}(T_0)$ seems to be a typing error in Ref 1 and should be replaced by $\sigma_{\mathrm{YS}}(RT)$.

[4]In the following, $T_{0,x}$ is used as a general term that includes T_0. The latter is regarded as a special case of the former for $x = 0$, i.e., $T_0 = T_{0,0}$.

types and sizes are used to be compared to each other, including 1*T*-CT specimens ($B = 25.4$ mm) and 3-point-bending specimens (SEB) of different sizes with square cross-sections ($W = B$), ranging from $B = W = 10$ mm (designated as 0.4T-SEB) to 80 mm (3.2T-SEB) (**Table 1**). The test specimens were machined from a forged ring of the not-commissioned German pressurized water reactor Biblis C, which is made of the RPV-steel 22 NiMoCr 3 7. A few 0.4T-SEB specimens (pre-cracked Charpy) were tested with a reduced crack-length of $a = 0.3$ W, to study the effect of reduced crack-tip constraints. To minimize the effect of material inhomogeneity, only the inner 2/3 of the wall thickness was used. In case of the SEB-specimens, half-sized specimens were machined from the broken halves of the bigger ones. The larger specimens were tested quasi-statically according to Ref 1. The 0.4T-SEB and 0.8T-SEB specimens were loaded at three different nominal rates as follows:

- "Quasistatic": 0.3 to 1.0 MPa$\sqrt{\text{m}}$/s, which is within the range as recommended in ASTM E1921-13 [1].
- "Medium": Crosshead speed of about 40 mm/s, leading to crack-loading rates of about $1.0 \cdot 10^4$ MPa$\sqrt{\text{m}}$/s.
- "Impact": Pre-cracked Charpy specimens loaded by an instrumented pendulum hammer with impact velocity of 2–2.5 m/s, which results in crack-loading rates of about $1.5 \cdot 10^5$ MPa$\sqrt{\text{m}}$/s for $a/W = 0.5$ and $3 \cdot 10^5$ MPa$\sqrt{\text{m}}$/s for $a/W = 0.3$, respectively.

The actual loading rate of each test series was determined after the tests as the first derivative of the $K_J(t)$ curve, with K_J denoting the stress intensity factor calculated from the J integral. It was found that the loading rate in terms of $\dot{K}_J$ was fairly constant in the range $K_J < 30$ MPa $\cdot$ m$^{0.5}$ for all specimens. This means that linear-elastic behavior prevails in this range, so $\dot{K}_J$ is the same as $\dot{K}_I$. Thus, the nominal loading rate could be determined from the initial slope of the load-vs.-time curve $F(t)$ by

$$\dot{K}_I = f(a) \cdot \frac{dF}{dt} \tag{4}$$

where:

$f(a)$ = the geometry factor in the general relation $K_I = f(a) \cdot F$.

TABLE 1 Used specimens and corresponding reference temperatures according to ASTM E1921 [1].

Specimen	Loading Rate	W (mm)	B (mm)	a/W	T_0, $T_{0,x}$ (°C)
CT	Static	50.8	25.4	0.5	−71
1.6T SEB	Static	40	40	0.5	−75.2
0.8T SEB	Static	20	20	0.5	−85.8
0.4T SEB	Static	10	10	0.5	−86.1
0.4T SEB 0.3	Static	10	10	0.3	−76.3
0.8T SEB	Medium	20	20	0.5	−32.5
0.4T SEB	Medium	10	10	0.5	−28.2
0.4T SEB	Impact	10	10	0.5	−11.7
0.4T SEB 0.3	Impact	10	10	0.3	−20.1

The static yield stress $R_{p0.2}$ as a function of temperature (in °C) was measured by standard tensile tests to be

$$R_{p0.2}(T) = 349 + 86.7 \cdot \exp(-0.00691 \cdot T) \quad \text{(in MPa)} \tag{5}$$

The dynamic yield stress R_{pd} at the loading rates corresponding to the impact tests was determined by rapid tensile tests as well as by instrumented Charpy tests. The latter were evaluated by means of the well-known relation between the yield stress and the yield force and maximum force in the Charpy test, as proposed originally by Server [11]. The empirical nondimensional factor 0.785 that appears in Server's relation was adjusted to 0.738 based on direct comparison between quasi-statically loaded Charpy specimen and the static tensile properties for the present material. In the temperature range of about $-80°C < T < 20°C$ the yield stress was found to be

$$R_{pd}[\text{MPa}] = 730.9 - 1.640 \cdot T[°C] \tag{6}$$

The K_{Jc} data of the quasi-static tests size-adjusted to $B = 24.5$ mm are shown in **Fig. 2**. The multi-temperature option of ASTM E1921 [1] was used to determine $T_{0,x}$. The results are listed in **Table 1**. The "best guess" value of T_0 is the one that was obtained from a relatively large number (about 20) of 1*T*-CT specimens, i.e., $T_0 = -71°$. Note that T_0 of 0.4T-SEB is 15 K lower, which corresponds to the "bias" mentioned in Ref 1. The MC shown in **Fig. 2** is calculated with the mean reference temperature $T_0 = -78°C$, which is obtained by considering all (approximately 100) data as one single set. As expected, most but a few of the individual data lay between the tolerance bounds corresponding to 5 % and 95 % probability of failure (p_f). Obviously, in an overall view, the data are consistent with the statistics behind Ref 1.

Shape of the Transition Curve

Table 1 includes the $T_{0,x}$ values determined according to Ref 1 from the tests at elevated loading rates. **Figure 3** shows the corresponding K_{Jc} data. In **Fig. 4**, the same data are shown size-

FIG. 2 Quasistatic K_{Jc} data measured by different specimens.

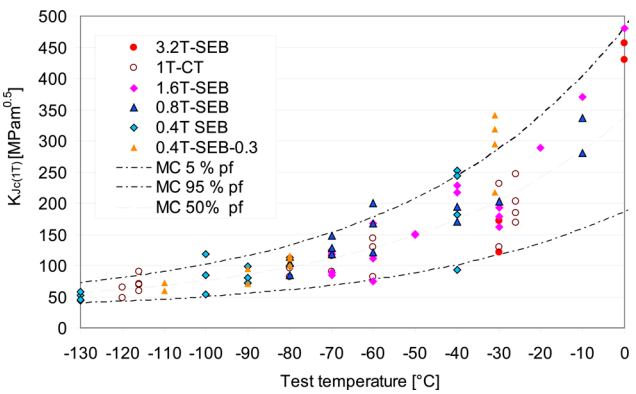

FIG. 3 K_{Jd} data obtained under increased loading rates as a function of test temperature.

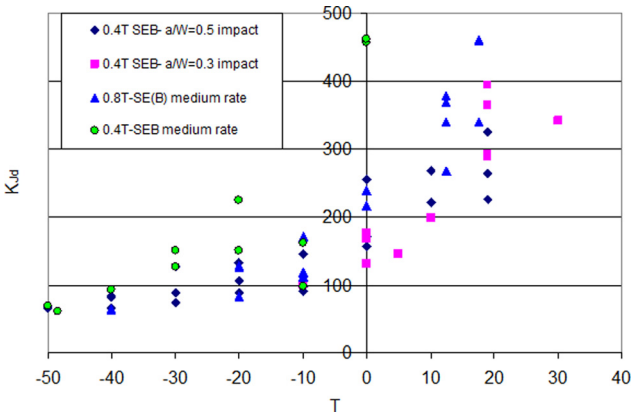

corrected and normalized by using $T - T_{0,x}$ as abscissa. By this normalization, the data from all tests should fall in one common scatter band described by the 5 % and 95 % tolerance bounds provided in Ref 1, like the static data did in **Fig. 2**. This is true for most of the valid data. However, as indicated by the dotted lines, the actual scatter band rises considerably steeper than the one described by the MC tolerance bounds, even within the window of validity according to Ref 1. This behavior is exhibited even clearer by the example of the K_{Jd} data from the 0.8T-SEB specimens under medium loading rate in comparison with the quasi-static K_{Jc} (**Fig. 5**). The general shape of the effective scatter bands shown in **Figs. 4** and **5** suggest that the DBT curves under elevated loading rate still follow an exponential function, but the corresponding exponent seems to be higher than 0.019. Thus, a function of the general form

$$K_{\mathrm{Jcmed}(1T)} = 30 + C \cdot \exp[p \cdot T] \tag{7}$$

where p and C are introduced as fitting parameters, and are expected to suit better than Eq 3 to fit the experimental data. Writing Eq 7 in the form

FIG. 4 Data from **Fig. 3**, corrected to $B = 25.4$ mm as a function of $T - T_{0,x}$, in comparison with the tolerance bounds of the MC.

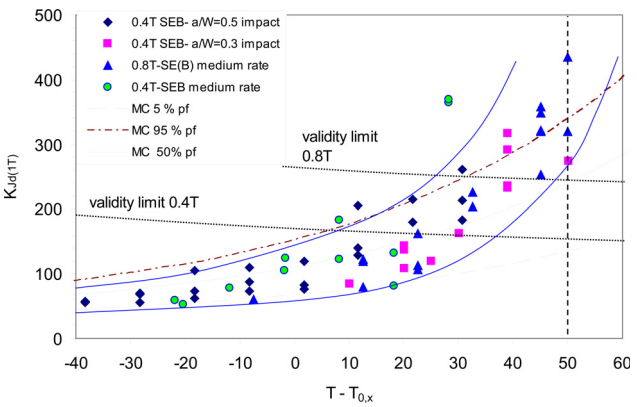

FIG. 5 Comparison between K_{Jc} measured on 0.8T-SEB-specimens quasi-statically and under medium loading rate with the trend predicted by the MC as a function of $T - T_{0,x}$.

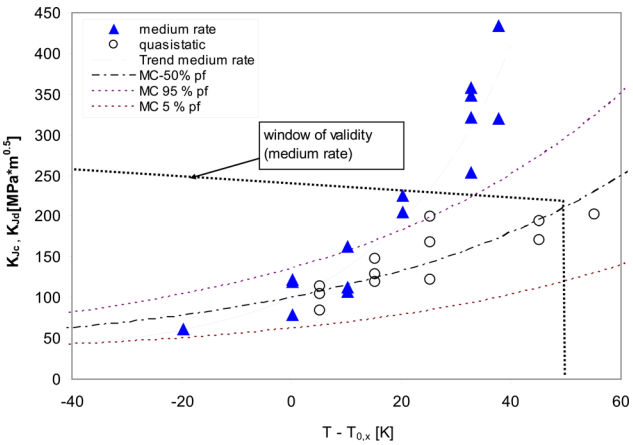

$$\ln(K_{\mathrm{Jcmed}(1T)} - 30) = \ln C + p \cdot T \tag{8}$$

shows that p and C can be obtained easily by linear regression of a sufficient number of $K_{Jc}(T)$ values in the diagram $\ln(K_{Jc} - 30)$ versus T. The values of p and C obtained in this way from the data shown in **Figs. 2** and **3** are listed in **Table 2**. At first, only the valid K_{Jc} (according to Ref 1) were used in the evaluation. Obviously, the p values exceed the standard value 0.019 in all but a few cases, particularly at elevated loading rates. For comparison, p values were also evaluated from all data of a test series, including the (non-censored) invalid ones. As can be seen from **Table 2**, inclusion of invalid data makes not much difference in p. This indicates that the trend described by Eq 7 continues with approximately the same p beyond the limit of validity.

In **Fig. 6**, the p values are shown as a function of the loading rate. Although the scatter is relatively large (which is not surprising with regard to the relatively few specimens in each data set), and despite a large data gap between quasi-static and

TABLE 2 Loading rates and values of p.

Specimen	Loading Rate (MPa$\sqrt{}$m/s)	p Valid Data Only	p Invalid Data Included
1T-CT	0.316	0.018	0.018
1.6T SEB	0.838	0.025	0.027
0.8T SEB	0.611	0.020	0.018
0.4T SEB	0.923	0.027	0.022
0.4T SEB 0.3	0.766	0.026	0.026
0.8T SEB	5700	0.042	0.043
0.4T SEB 0.5	7018	0.030	0.042
0.4T SEB 0.5	150 000	0.028	0.029
0.4T SEB 0.3	300 000	0.041	0.043

FIG. 6 Exponent p as a function of loading rate. The dotted line represents the estimated trend.

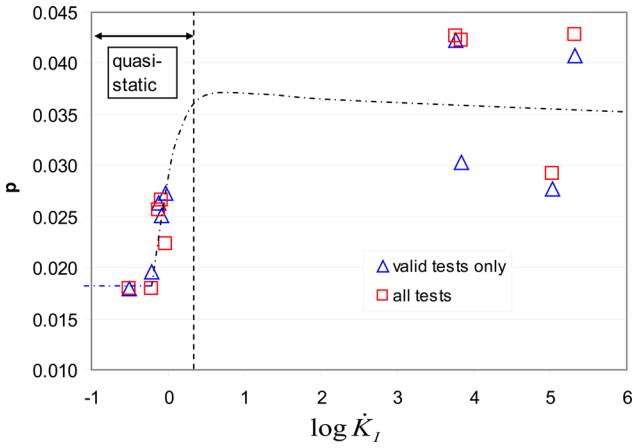

medium loading rates, the trend is quite clear. A steep rise in the upper part of the quasi-static range (which is defined as 0.1 MPa · m$^{0.5}$/s $< \dot{K}_I <$ 2 MPa · m$^{0.5}$/s in Ref 1, followed by a saturation at a level of about $p = 0.03$–0.04 for higher loading rates. A physical explanation for this sigmoidal behavior is given later, as well as further experimental evidence.

It is evident that the evaluation procedure of Ref 1 becomes inaccurate if p deviates from 0.019 and the test temperature differs from $T_{0,x}$. This problem can be overcome by using the "open exponent fit" (OEF) method, as described in the next section.

Reference Temperature t_{100}

By definition, $T_{0,x}$ is the temperature at which $K_{Jc(\mathrm{med},1T)}$ takes the value of 100 MPa · m$^{0.5}$ [1]. If p in Eq 7 differs from 0.019, then $T_{0,x}$ determined according to Ref 1 has no longer this physical meaning. For these cases, we introduce a generalized reference temperature, denoted as $T_{100,x}$, that is defined by

$$K_{Jc(\mathrm{med},1T)} = 30 + 70 \cdot \exp\left[p \cdot (T - T_{100,x})\right] \tag{9}$$

Obviously, $T_{100,x}$ is identical with $T_{0,x}$ if $p = 0.019$, but deviates from $T_{0,x}$ if p deviates from 0.019. In the latter case, $T_{100,x}$ is expected to be more precise and physically meaningful as a reference temperature than $T_{0,x}$. In applications like a failure analysis of a structural component, $T_{100,x}$ has the same physical meaning as $T_{0,x}$ and can replace the latter.

With $K_{Jc(\mathrm{med},1T)} = 100$ MPa · m$^{0.5}$ (Eq 8) leads to

$$T_{100,x} = \frac{4.2485 - \ln C}{p} \tag{10}$$

Graphically, the determination of $T_{100,x}$ is illustrated in **Fig. 7**, as an example. Inserting the values of p and C from **Table 2** in Eq 10 results in the $T_{100,x}$ values contained in **Table 3**, where they

FIG. 7 Determination of C, p, and $T_{100,x}$ by linear regression, shown by the example of quasi-statically loaded 1T-CT specimens.

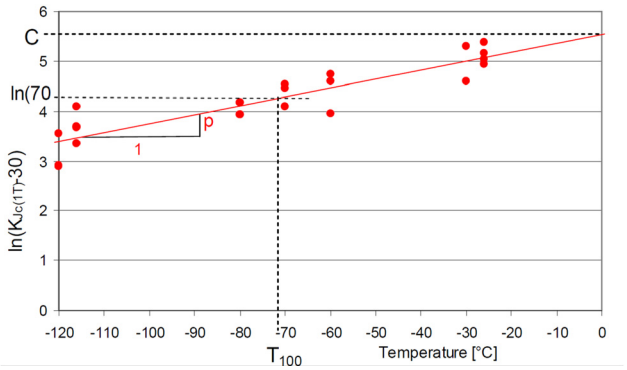

are compared with the standard $T_{0,x}$. The differences between $T_{0,x}$ and $T_{100,x}$ appear to be stochastic, ranging from −6 K to +7 K for quasi-static tests and up to 14 K for the dynamic tests. As shown in the next section, this behavior is theoretically explicable. Anyway, it can contribute significantly to the uncertainty of $T_{0,x}$ as given in Ref 1. In case of single-temperature testing at a temperature relatively far from $T_{0,x}$, the differences between $T_{0,x}$ and $T_{100,x}$ can be much larger than those in **Table 3**, as discussed below.

For comparison, **Table 3** contains $T_{100,x}$ that are obtained by using not only the "valid" K_{Jc} data (according to the qualification criteria of Ref 1, but all data of each test series, including several non-censored "invalid" ones. In an overall view, $T_{100,x}$ obtained from the unrestricted data sets are nearly the same as those from just the valid data. This indicates that the validity criteria for individual K_{Jc} data can probably be relaxed if the OEF method is used. This issue is dealt with later.

Effect of Test Temperature on $T_{0,x}$

In cases where p is significantly higher than 0.019, the main influencing factor on the deviation between $T_{0,x}$ and $T_{100,x}$ is

TABLE 3 Comparison between $T_{0,x}$ and $T_{100,x}$.

		$T_{100,x}$ (°C)			
Specimen	Loading Rate (MPa$\sqrt{}$m/s)	Valid Data Only	From all Data	$T_{0,x}$ (°C) ASTM E1921 [1]	$T_{100,x}$ - $T_{0,x}$ (K) (Valid Data)
1T-CT	0.316	−72.8	−73.3	−71	−0.83
1.6T SEB	0.838	−68.0	−67.6	−75.2	7.16
0.8T SEB	0.611	−85.2	−82.7	−85.8	0.62
0.4T SEB	0.923	−82.7	−81.6	−86.1	3.43
0.4T SEB 0.3	0.766	−82.4	−82.8	−76.3	−6.13
0.8T SEB	5700	−20.2	−20.2	−32.5	12.27
0.4T SEB 0.5	7018	−28.3	−28.3	−28.2	−0.10
0.4T SEB 0.5	150 000	−6.4	−14.9	−11.7	5.31
0.4T SEB 0.3	300 000	−5.9	−6.4	−20.1	14.17

FIG. 8 Dependence of T_0 on the test temperature T^A_{test} and T^B_{test} in case of $p > 0.019$ (schematically).

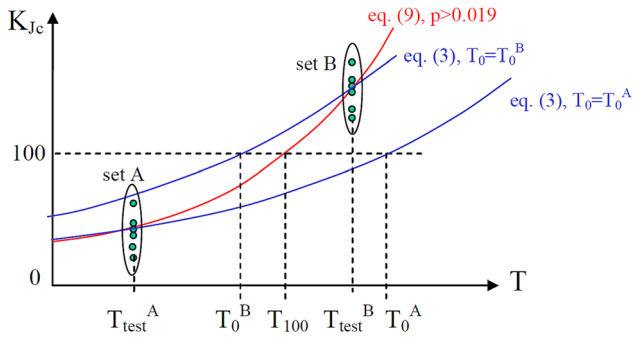

the difference between the test temperature T_{test} and the reference temperature $T_{100,x}$. In **Fig. 8**, the corresponding effect is illustrated schematically, for the sake of simplicity just for quasi-static loading ($x = 0$), thus $T_{0,0} = T_0$ and $T_{100,0} = T_{100}$. We consider a case where the median $K_{Jc(med,1T)}(T)$ is given by Eq 9 with $p > 0.019$ (red line in **Fig. 8**). Correspondingly, the correct reference temperature is T_{100}. If a set of minimum six specimens (set A) is tested by the single specimen option at a temperature $T^A_{test} < T_{100}$, then the procedure according to Ref 1 results in the reference temperature T^A_0. If another set of specimens (set B) is tested at a temperature $T^B_{test} > T_{100}$, then a different reference temperature $T^B_0 < T_{100}$ is obtained by the procedure of Ref 1. If both series are evaluated in combination, then T_0 will be in between T^A_0 and T^B_0, thus closer to the true value T_{100}. Only in the unlikely case of T_{100} - T^A_{test} and T^B_0 - T_{100} being equal the procedure of Ref 1 delivers the correct result $T_0 = T_{100}$.

On the other hand, the OEF method gives the correct result for any choice of T^A_{test} and T^B_{test}, provided a sufficient number of specimens are tested at both temperatures. Obviously, single-temperature testing is not possible when using the OEF method. However, splitting a given set of say six to eight specimens in two halves, and testing one at T^A_{test} and the other at T^B_{test} enables T_{100} to be determined with reasonable accuracy.

In mathematical terms, the influence of T_{test} and p on $T_{0,x}$ can be easily derived from Eq 10, using the fact that $T_{100,x} = T_{0,x}$ for $p = 0.019$, which follows from Eqs 9 and 3. One obtains

$$T_{0,x} - T_{100,x} = (T_{test} - T_{100,x}) \cdot \left(1 - \frac{p}{0.019}\right) \quad (11)$$

According to Eq 11, the difference $T_{0,x}$ - $T_{100,x}$ can be as large as 50 K, if the loading rate is such that p is on the order 0.03 and single-temperature tests are performed at test temperatures close to the ±50 K limit set by Ref 1. If the multi-temperature option of Ref 1 is used, then estimates of $T_{0,x}$ - $T_{100,x}$ can be obtained by averaging the results of Eq 11 for the different test temperatures.

In the present test program, the test temperatures T_{test} were chosen rather arbitrarily, but not too far from $T_{0,x}$. In all cases, they were located on both sides of $T_{0,x}$. This is the explanation for why the deviations between $T_{0,x}$ and $T_{100,x}$ in **Table 3** are in general not very big, and positive as well as negative. By testing at a single temperature relatively far from $T_{0,x}$, the differences would have been much larger, as it can be seen from Eq 11.

Effect of Loading Rate on Reference Temperature

Figure 9 shows $T_{0,x}$ of the tests at elevated loading rates as a function of the loading rate in comparison with the prediction provided by Eqs 2*a* and 2*b*. The prediction is improved if not T_0 from the 0.4T-SEB, but from the CT-specimens is inserted in Eq 2*b*. In addition, $T_{0,x}$ data determined recently by Böhme et al. [12,13] for the same steel at high loading rates are included in **Fig. 9**. Most of these $T_{0,x}$ are significantly higher than predicted by Eq 2*a*, even if T_0 is chosen to be as high as possible ($T_0 = -71°C$, according to **Table 2**).

Furthermore, it was found that Eqs 2*a* and 2*b* agree better with $T_{0,x}$ than with $T_{100,x}$, although the latter are expected to be more accurate. Probably, the p-effect discussed above corrupted many of the experimental data behind the empirical relation 2*b*, so the latter is also corrupted. Anyway, determination of a similar correlation formula as 2*a* based on the more accurate $T_{100,x}$ values is expected to be preferable. As shown in Refs 2 and 5, the theory of thermal activation of plastic flow [14,15] applied to crack-initiation leads to the general relation

$$T_{100,x}[K] \cdot \ln \frac{\dot{K}_0}{\dot{K}_I} = \text{const} \quad (12)$$

Using Eq 12 to fit a regression line between the best estimate $T_{100,x}$ (−71°C, according to the discussion above) and the $T_{100,x}$

FIG. 9 $T_{0,x}$ at elevated and high loading rates, compared with data from Böhme et al. [12] and the prediction of Eqs. 2*a* and 2*b*.

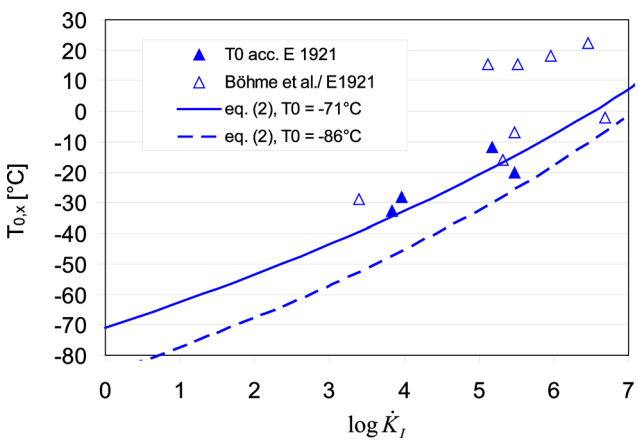

values obtained from the 0.4T-SEB specimens at increased loading rates results in

$$T_{100,x}[^\circ\mathrm{C}] = \frac{4517}{22.37 - \log \dot{K}_I} - 273 \quad (13)$$

Equation 13 is shown as the dashed line in **Fig. 10**. This relation surely holds only for the considered RPV-steel, because rate effects are known to depend on the yield stress. With the yield stress at room temperature from Eq 5, Eq 1 predicts a shift of $\Delta T_{R\&B} = 68.8$ K between the static loading and the rate corresponding to a standard Charpy test. Comparison with Eq 13 reveals that this temperature shift corresponds to $\dot{K}_I = 4.45 \cdot 10^5$ MPa · m$^{0.5}$/s (**Fig. 10**), or in mathematical terms:

$$T_{100} + \Delta T_{R\,B} = T_{100,x}(\dot{K}_I = 4.45 \times 10^5\ \mathrm{MPa} \times \mathrm{m}^{0.5}/\mathrm{s}) \quad (14)$$

In fact, $\dot{K}_I = 4.45 \cdot 10^5$ MPa · m$^{0.5}$/s corresponds roughly to the loading rate of a Charpy test, if the standard notch is interpreted as a crack of length $a_0 = 2$ mm [2]. This means that Eq 13 is fairly consistent with Eq 1, so the latter can be used to generalize Eq 13. Inserting Eq 14 in 12 and using 1 leads to

$$T_{100,x}[^\circ\mathrm{C}] = \frac{T_{100} + 273}{1 - \dfrac{21.1 - 0.0213 \cdot R_{p0.2}}{T_{100} + 392 - 0.12 \cdot R_{p0.2}} \cdot \log \dot{K}_I} - 273 \quad (15)$$

where:

$R_{p0.2}$ = the yield stress at room temperature (in MPa). Alternatively, Eq 15 can be rearranged to match formally with $2a$, which enables Γ as introduced in $2a$ to be obtained as

$$\Gamma = \frac{T_0 - 0.12 \cdot R_{p0.2} + 392}{48.28 - 0.0487 \cdot R_{p0.2}} \quad (16)$$

Inserting Eq 16 in $2a$ is equivalent to 15. Note that in Eq 16, T_{100} is replaced by T_0, to be comparable with $2b$. Switching between T_0 and T_{100} in the relations 12–16 is consistent, because T_{100} and T_0 have the same physical meaning. Thus, in Eqs 12–16, $T_{100,x}$ or T_{100} can be replaced by $T_{0,x}$ and T_0, respectively, and vice versa.

Note that Eq 16 performs at least as well as $2b$ to estimate $T_{0,x}$, by $2a$, although it is based on just three experimental $T_{100,x}$ values (discussed later). Corresponding to footnote 3, the agreement between Eqs $2b$ and 16 is improved if the yield stress at room temperature is inserted in $2b$ instead of the one at T_0. With this modification, the predictions of Eqs $2a$ and $2b$ agree with 15 quite well in the entire range of yield strengths that is covered by Ref 1. Regarding the completely different way of their derivation and the fact that Eq 15 is based on just three experimental $T_{100,x}$ values of a single material, the good agreement is amazing and another indication for the superiority of $T_{100,x}$ at increased loading rates.

FIG. 10 Regression line (13) based on $T_0 = -71°$ and $T_{100,x}$ of 0.4T-SEB-specimens at elevated loading rates, compared with Eqs 1 and 2.

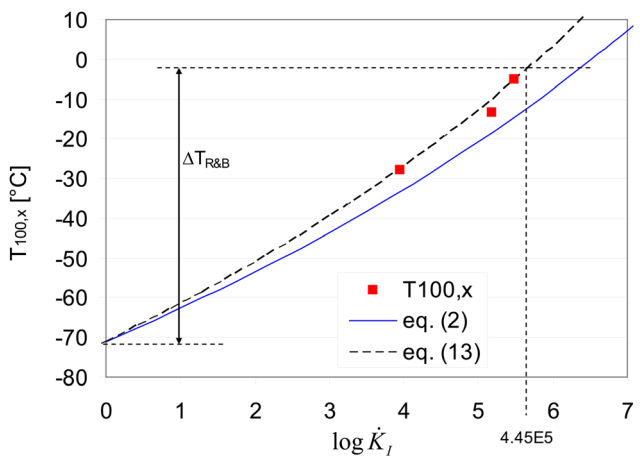

Discussion

PHYSICAL EXPLANATION FOR THE DISTORTION OF THE TRANSITION CURVE

The exponential increase of fracture toughness in the DBT range, which is reflected by Eqs 3 or 7, can be explained by the mechanism of initiation of cleavage [6,16]. It results from the interaction by positive feedback between fracture toughness, plasticity, and crack-tip constraints as follows. As the test temperature increases, the yield stress decreases, which leads to increasing plasticity at the crack tip, causes the crack-tip constraints to decay [17], results in higher toughness, promotes plastic yielding, and further reduction of constraints, and so on. If the loading rate is increased, then the temperature produced by energy dissipation remains partly in the material in the vicinity of the crack front as an adiabatic heating, which accelerates the processes described above. Furthermore, the local heating of the plastic zone may cause temperature-induced compressive stresses in the process zone, which accelerates the loss of constraints. Thus, an increase of p with increasing loading rate appears to be physically explicable and plausible. At high loading rates, however, effects of rate-induced embrittlement caused by the strain-rate dependence of the yield stress interfere more and more with the interactions described above. This leads to a reduced plastic yielding and, consequently, to lower adiabatic heating with increasing loading rate. The combination of these two competing effects results in the observed sigmoidal trend of $p(\dot{K}_I)$ shown in **Fig. 6**.

COMPARISON WITH INDEPENDENT EXPERIMENTAL DATA AT HIGH RATES

The data from tests under very high loading rates performed by Böhme et al. [12,13] are well suited for an independent validation and an extension to higher rates of the presented relations. The corresponding $T_{0,x}$ values are included in **Fig. 9**. Because

these data are obtained by single-temperature tests, the direct application of the OEF method is not possible. However, if p was known, $T_{100,x}$ could be obtained from $T_{0,x}$ by means of Eq 11.

To determine p independently from **Fig. 6**, the experimental data of Refs 12 and 13 are plotted in **Fig. 11** in the diagram $T_{0,x} - T_{100,x}$ versus T_{test} - $T_{100,x}$. Because the corresponding $T_{100,x}$ are unknown, auxiliary values obtained from Eq 15 are used as dummies. According to Eq 11, the data should form a straight line with a negative slope, the latter being related to p. Note that the slope in question does not depend on the dummy $T_{100,x}$, because the latter appears on both the abscissa and the ordinate in **Fig. 11**. Although the scatter of the data shown in **Fig. 11** is relatively large—which is not surprising regarding the different specimen types, sizes, and loading techniques behind the data of Refs 12 and 13—there is a clear trend to higher $T_{0,x}$ with lower T_{test} - $T_{100,x}$, as predicted by Eq 11 for $p > 0.019$. Based on Eq 11, p can be calculated from the slope s of the corresponding regression line, which is $s = 0.530$. With Eq 11, one finds $p = 0.019 \cdot (1 - s) = 0.029$. The fact that the regression line crosses nearly perfectly the origin of the diagram (**Fig. 11**) indicates that Eq 15 delivered consistent $T_{100,x}$, which confirms Eq 15, because incorrect dummy values of $T_{100,x}$ would have caused a parallel shift of the regression line away from the origin.

The value $p = 0.029$ as found above fits well to the trend shown in **Fig. 6** for higher rates. By using this value in Eq 1, $T_{0,x}$ from Refs 12 and 13 can be transferred to $T_{100,x}$. The results are shown in **Fig. 12**. Obviously, compared to **Fig. 9**, the scatter is dramatically reduced. Furthermore, the $T_{100,x}$ values are below the reference temperature for crack arrest, T_{KIa}, whereas some of the original $T_{0,x}$ were located beyond it, which is hardly possible (see Ref 18] for further discussion). Overall, the corrected $T_{100,x}$ shown in **Fig. 12** are much more plausible than the original $T_{0,x}$ shown in **Fig. 9**.

FIG. 11 Theoretical relation between $T_{0,x}$ - $T_{100,x}$ and T_{test} - $T_{100,x}$ for three exemplary values of p, compared with experimental data from Böhme et al. [12] and the corresponding linear regression.

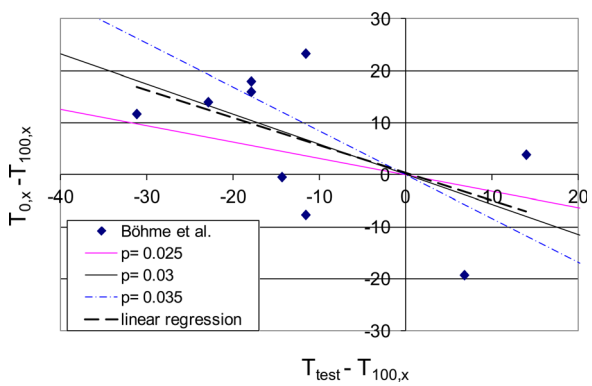

FIG. 12 $T_{100,x}$ from Böhme et al. [12] evaluated with $p = 0.029$ and $T_{100,x}$ of the present investigation at increased loading rates, in comparison with the predictions of Eqs 15 and 2.

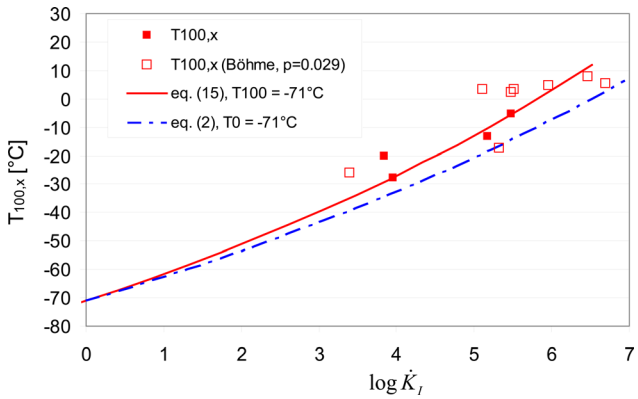

As far as Eq 15 is concerned, it agrees well with the corrected $T_{100,x}$ data shown in **Fig. 12**. It tends to perform better than Eq 2*a* to predict $T_{100,x}$ or $T_{0,x}$ from T_0.

VALIDITY OF $T_{100,x}$

The validity criteria for $T_{0,x}$ according to Ref 1 reflect not only issues of transferability but also aspects associated with the evaluation procedure. The latter is different in case of $T_{100,x}$, so the corresponding criteria should be revisited.

From the examples shown in **Figs. 4** and **5** one can see that $K_{Jc}(T)$ form a scatter band of the exponential shape (Eq 7) even beyond the validity limits according to Ref 1. Thus, a curve of form 7 can still be fitted through these data, irrespective of the individual validity of K_{Jc}. Actually, K_{Jc} data outside the validity window of Ref 1 still can carry valuable information to determine p and C (which can be size dependent), as long as there is only minor stable crack extension prior to cleavage. For the resulting $T_{100,x}$, validity of the individual K_{Jc} values for $T > T_{100,x}$ does not matter, as long as K_{Jc} at $T \leq T_{100,x}$ are valid. Indeed, comparing the values of $T_{100,x}$ resulting from partly invalid data with those from valid data only (**Table 3**) exhibits few differences.

According to the above considerations, the K_{Jc} value that corresponds to the reference $K_{Jc} = 100\ \mathrm{MPa \cdot m^{0.5}}$ for a standard $1T$ specimen (i.e., thickness 0.0254 m), which for the actual specimen thickness B is equivalent to

$$K_{Jc}[\mathrm{MPa} \times \mathrm{m}^{0.5}] = 20 + 80 \cdot \left(\frac{0.0254}{B[\mathrm{m}]}\right)^{0.25} \tag{17}$$

needs to be valid at $T = T_{100,x}$. According to Ref 1, this is the case if

$$\sqrt{\frac{E \cdot b_0 \cdot R_{p0.2}^{T=T_{100,x}}}{30 \cdot (1-\nu^2)}} > 20 + \frac{31.94}{B^{0.25}} \tag{18}$$

Correspondingly, obtaining a valid $T_{100,x}$ is principally possible for specimens that fulfill the criterion

$$b_o \geq \left(20 + \frac{31.94}{B^{0.25}}\right)^2 \cdot \frac{30 \cdot (1-\nu^2)}{E \cdot R_{p0.2}^{T=T_{100,x}}} \quad (19)$$

In Eq 19, B and b_0 have to be inserted in meters, E and $R_{p0.2}$ in MPa. In case of increased loading rates ($x > 0$), the dynamic yield stress according to Ref 1 should be used as $R_{p0.2}$. Note that K_{Jc} of the individual tests do not appear in criterion 19. This makes sense physically and is a remarkable advantage of the OEF method, compared with the standard evaluation according to Ref 1. It means that validity of $T_{100,x}$ is just a question of choosing a sufficiently large specimens, and not of the individual K_{Jc}, as far as fracture is triggered by cleavage. It enables valid $T_{100,x}$ to be obtained even from datasets that are insufficient for the evaluation of a valid $T_{0,x}$.

Conclusions

The experimental data obtained from tests on a representative RPV steel clearly show that the transition curve at increased loading rates is significantly steeper than under quasi-static loading. This effect starts to appear even at rather slow rates of about $\dot{K}_I > 1\,\text{MPa}\cdot\text{m}^{0.5}/\text{s}$. In the range of quasi-static loading, the effect on T_0 is in general rather minor. It can be minimized by using the multi-temperature option of Ref 1 and testing at temperatures as close to T_0 as possible, which can be achieved by an iterative testing scheme.

However, at increased loading rates effect of the increased p on T_0 can be significant. For medium and high rate loading the coefficient p seems to saturate at a value of about 0.03. Consequently, the evaluation procedure of ASTM E1921 [1], where p is presumed to be 0.019, leads to an additional uncertainty of $T_{0,x}$ at elevated loading rates. It causes $T_{0,x}$ to be biased by the test temperature, which enables $T_{0,x}$ to be manipulated by the corresponding choice. If the test temperature is considered to be arbitrary, then this bias increases the uncertainty and the apparent scatter of the measured $T_{0,x}$.

These problems can be avoided by using the OEF method as described above to determine the reference temperature $T_{100,x}$, provided that a K_{Jc} dataset with a good spreading on the temperature axis is available. Moreover, the OEF method offers advantages concerning qualification of the data. Even "invalid" K_{Jc} can be used without censoring as auxiliary points to define the required regression line, provided a few valid data relatively close to T_0 are available. Because there is no need for censoring, there is no need for a costly determination of the yield stress at high strain rates. Because of the reduced uncertainty of $T_{100,x}$, compared with $T_{0,x}$, the OEF method is preferable to study the effects of potentially influencing factors on T_0, like the rate effect by Eq 15 or the thickness effect in Refs 7 and 8.

The precision and applicability of ASTM E1921 [1] could be significantly improved by accounting for these findings in a suitable way. Whether or not a given dataset is well suited for an evaluation by the OEF approach depends on the spreading and distribution of the K_{Jc} data on the temperature axis. However, considering the advantages of the method in some cases, particularly for increased loading rates, the OEF method as described above should be considered as an option in Ref 1.

References

[1] ASTM E1921-13: Standard Test Method for Determination of Reference Temperature, T_0, for Ferritic Steels in the Transition Range, *Annual Book of ASTM Standards*, ASTM International, West Conshohocken, PA, 2013.

[2] Schindler, H. J. and Morf, U., "Toughness Testing and Assessment of Welds," *Proceedings of the International Conference on Engineering Design in Welded Constructions*, Madrid, Spain, Sept 7–8, 1992.

[3] ASTM E23-12: Method for Notched Bar Impact Testing of Metallic Material, Charpy-Test, *Annual Book of ASTM Standards*, ASTM International, West Conshohocken, PA, 2012.

[4] Rolfe, T. H. and Barsom, J. M., *Fracture and Fatigue Control in Structures: Applications of Fracture Mechanics*, Prentice-Hall, Englewood Cliffs, NJ, 1977.

[5] Wallin, K. and Planman, P., "Effect of Strain Rate on the Fracture Toughness of Ferritic Steel," *IAEA Specialists Meeting*, Paper No. 17, Prague, Czech Republic, Sept 2001.

[6] Schindler, H. J., Kalkhof, D., and Tipping, P., "Determination of Transferable Lower-Bound Fracture Toughness from Small Specimens," *J. ASTM Int.*, Vol. 5, No. 8, 2008, JAI101168.

[7] Schindler, H. J. and Kalkhof, D., "Lower Bounds and Saturation Effects of Dynamic Fracture Toughness in the Ductile-to-Brittle Transition Regime of Ferritic Steel," Transactions, SMiRT-22, Division II, San Francisco, CA, 2013.

[8] Kalkhof, D. and Schindler, H. J., "Uncertainties in T_0 and Corresponding Safety Margins in Lower Bounds of K_{Ic} in the Ductile-to-Brittle Transition Regime of Ferritic Steels," *Paper ID 257, Proceedings of the 19th European Conference on Fracture*, Kazan, Russia, Aug 26–31, 2012.

[9] Zurbuchen, C. and Viehrig, H. W., "Bruchmechanische Werkstoffcharakterisierung zur Überwachung der Neutronenversprödung von Reaktordruckbehältern [Fracture mechanics characterisation of materials in irradiation embrittlement surveillance of reactor pressure vessels]," Forschungszentrum Dresden, Institutsbericht FZD/FWS/2009/07, Sept 2009.

[10] Viehrig, H. W., Zurbuchen, C., Schindler, H. J., and Kalkhof, D., "Effects of Test Parameters on the Master Curve Reference Temperature," *18th European Conference on Fracture (ECF 18)*, Dresden, Germany, Aug 30–Sept 3, 2010.

[11] Server, W. L., "General Yielding of Charpy-V-Notch and Precracked Charpy Specimens," *J. Eng. Material Technol.*, Vol. 100, 1978, pp. 183–188.

[12] Böhme, W. Mayer, U., "Überprüfung und Weiterentwicklung von Bewertungs-methoden für dynamische Rissinitiierung und Rissarrest [Verification and further development of assessment methods for dynamic crack initiation and crack arrest]„" Project No. 150 1368, *Report No. 665/2012*, IWM, Freiburg, Germany, 2012.

[13] Böhme, W., Reichert, T., and Mayer U., "Assessment of Dynamic Fracture Toughness Values K_{Jc} and Reference

Temperatures $T_{0,x}$ Determined for a German RPV Steel at Elevated Loading Rates According to ASTM E1921," SMiRT 22, San Francisco, CA, 2013.

[14] Priest, A. H., "Influence of Strain Rate and Temperature on the Fracture and Tensile Properties of Several Metallic Materials," *Dynamic Fracture Toughness*, The Welding Institute, Cambridge, U.K., 1977.

[15] Krabiell, A. and Dahl, W., "Zum Einfluss von Temperatur und Dehngeschwindigkeit auf die. Streckgrenze von Baustahlen unterschiedlicher Festigkeit," *Archiv für das Eisenhüttenwesen*, Vol. 52, 1981, pp. 426–436.

[16] Anderson, T. L., *Fracture Mechanics: Fundamentals and Applications*, 3rd ed., CRC, Boca Raton, FL, 2005.

[17] Kim, Y. J., Kim, J-S., Cho, S-M., and Kim, Y-J., "3-D Constraint Effects on J Testing and Crack Tip Constraint in M(T), SE(B), SE(T) and C(T) Specimens: Numerical Study," *Eng. Fract. Mech.*, Vol. 71, 2004, pp. 1203–1218.

[18] Schindler, H. J. and Kalkhof, D., "Lower Bounds and Saturation Effects of Dynamic Fracture Toughness in the Brittle-to-Ductile Transition Regime of Ferritic Steels," Transactions, SMiRT-22, Division II, San Francisco, CA, 2013.